Direct Laser Writing of Crystallized TiO 2 and TiO 2 /Carbon Microstructures with Tunable Conductive Properties

Shang-Yu Yu, Gautier Schrodj, Karine Mougin, Joseph Dentzer, Jean-Pierre Malval, Hsiao-Wen Zan, Olivier Soppera, Arnaud Spangenberg

DOI: 10.1002/((please add manuscript number))
Article type: Communication

Direct Laser Writing of Crystallized TiO_2 and TiO_2/Carbon Microstructures with Tunable Conductive Properties

Shang-Yu Yu, Gautier Schrodj, Karine Mougin, Joseph Denzer, Jean-Pierre Malval, Hsiao-Wen Zan, Olivier Soppera, Arnaud Spangenberg**

S-Y. Yu, G. Schrodj, Dr. K. Mougin, Dr J. Denzer, Dr J-P. Malval, Dr. O. Soppera, Dr. A. Spangenberg
Université de Haute-Alsace, CNRS, IS2M UMR 7361, F-68100 Mulhouse, France
Université de Strasbourg, France
E-mail: olivier.soppera@uha.fr; arnaud.spangenberg@uha.fr

Prof. H.-W. Zan
Department of Photonics, College of Electrical and Computer Engineering, National Chiao Tung University, Hsinchu, Taiwan 30010, Republic of China

Keywords: femtosecond direct laser writing, functional metal oxide, conductive micropattern, TiO_2 / carbon nanocomposite, miniaturized pressure sensor

Abstract

Metal oxides are an important class of materials for opto-electronic applications. In this context, developing simple and versatile processes for integrating these materials at the microscale and nanoscale has become increasingly important. One of the major remaining challenges is to control the microstructuration and electro-optical properties in a single step. We show here that near-infrared femtosecond laser irradiation can be successfully used to prepare amorphous or crystalized TiO_2 microstructures in a single step using a direct laser writing approach from a TiO_2 precursor thin film doped with a suitable dye. When laser writing is conducted under a nitrogen atmosphere, simultaneous to the crosslinking of the Ti-oxide precursor, the graphitization of the organic species embedded in the initial film is observed. In this case, a carbon network is generated within the TiO_2 matrix, which significantly increases the conductivity. Moreover, the TiO_2/C nanocomposite exhibits piezoresistive behavior that was used in a pressure sensor device. Using this route, it is possible to use direct laser writing to fabricate microsized pressure sensors.

Metal oxides (MOs) have emerged as important functional materials for the design of devices that are used in a broad range of applications, such as health monitoring, electronic skin, displays or solar cells, among others.[1-4] Among all MOs, ZnO, TiO_2, ZrO_2, and HfO_2, in particular, are attractive due to their excellent optical properties (transparency in the visible range and high refractive index) combined with electronic properties for use in conductors, semiconductors, and insulators.[5] Electronic properties are indeed closely linked to the nature of the metal and conditions of fabrication, which determine the structure of the final material at the atomic scale. These properties can be modified by doping with different metals, by adjusting the metal to oxygen stoichiometry or by generating an amorphous or crystal phase. [6-9]

Today, integration of MOs as thin films, micro-patterns or nano-patterns by convenient and simple means remains a major challenge for the fabrication of electronic and optoelectronic devices. MOs are commonly deposited as thin films by sputtering. Though the sputtered MOs usually exhibit better electrical properties due to the accurate control of the composition and defect concentration at the atomic scale, solution-based processes have gained much attention during the last years due to their simplicity, cost-effectiveness, vacuum-free processes and high versatility.

In solution-based processes, thermal annealing is required to eliminate the solvent and organic ligands that are complexed on metal ions and to obtain material and phase compositions with suitable properties. This step is typically conducted at temperatures ranging from 300°C to 1000°C. Thus, such a fabrication strategy can be difficult to apply in the case of multistep integration processes involving different materials.

In this context, laser processing of MOs presents many advantages due to the control of the laser-matter interaction in space and time.[9] Laser curing allows a fast treatment that can be confined to a limited volume by focusing the laser beam. Such a laser- induced effect leads to a much lower energy consumption with respect to that of thermal annealing. For example, a

pulsed laser in the ultra-violet (UV) or near-infrared (NIR) range has been successfully used for the crystal growth of amorphous MO films [10, 11] or the hydrothermal growth of MO nanostructures.[12, 13]

Recently, laser processing has also been introduced for the direct writing of MO microstructures. For this purpose, UV or Deep-UV (DUV) wavelengths are usually used. At the molecular scale, the patterning proceeds according to the photo-decomposition of the metal precursors complexed by organic molecules. Patterning can be obtained at room temperature down to the nanoscale using direct laser writing (DLW), but usually, a thermal post-treatment is needed to obtain an MO with suitable optical or electrical properties.[6-8, 14, 15] For example, Yeh et al. have shown that laser irradiation of a zinc oxide (ZnO) sol-gel based photoresist using DUV lithography can produce nanostructures.[16] However, the resulting amorphous material exhibits a limited electrical performance. Nevertheless, after 1 hour of thermal annealing at 500°C, the field-effect mobility increased from 0.0075 $cm^2.V^{-1}$ to 0.034 $cm^2.V^{-1}$, which was attributed both to the elimination of the organic residue inside the original photoresist and to the crystallization of ZnO. Kim et al. have also demonstrated that DUV irradiation combined with moderate heating (150°C) allows for suppression of thermal annealing post-treatment while preserving the final performance of the MO.[1] However, the feasibility of performing such a strategy for micropatterning has not been explored. In another study, TiO_2 sol-gel precursors were directly excited by femtosecond laser pulses at 800 nm through a multiphoton process. The authors showed that the modification was strongly correlated to the laser fluence. However, no investigation of the resulting material was performed and thermal curing was needed to obtain the crystallized material.[17]

In the present work, we propose a new strategy combining photothermal and photochemical activation of TiO_2 sol-gel precursors using femtosecond NIR direct laser writing. TiO_2 was chosen due to its potential as a transparent, highly refractive material with semi-conducting properties. TiO_2 has shown great performance in opto-electrical applications (micro-optics,

MEMS devices, dye-sensitized solar cells, electrochemical sensors, and photocatalysts).[18-21] For practical applications, a simple means of integrating TiO_2 with a crystallinity control is needed.[22]

We show that our strategy allows for the fabrication of micropatterned crystallized TiO_2 in a single step under air and at room temperature. Activation of the TiO_2 sol-gel precursor is efficiently triggered under a 2-photon absorption mechanism by a photoabsorber added in the metal oxide precursor solution. The laser induced chemical modification was investigated by coupling photostructuration experiments and Raman microspectroscopy. Remarkably, by adjusting the laser fluence and surrounding atmosphere, we also show the ability to tune the electrical properties via *in situ* generation of disordered carbon, leading to a novel and easy method for integrating TiO_2/carbon composites in microdevices. As a proof of concept, electrical characterization of TiO_2/carbon microstructures is performed, and an application as a miniaturized pressure microsensor is shown in the last section.

Figure 1 presents a schematic view of the fabrication process of microstructures using femtosecond DLW for titanium precursor solutions and their application as a pressure sensor. The first step is the solution preparation. A commercial titanium precursor (titanium isopropoxide) was mixed with methacrylic acid in 1-propanol. Carboxylic acids are commonly used as stabilizers of transition metals since they can form strong bonds with metals. After 24 hr of stirring in an acid environment, a stable solution was obtained. The solution preparation conditions were chosen to limit the condensation reaction of the titanium precursor. The excess complexing agent associated with the presence of water was shown to lead to metal-oxo clusters (MOC) in the solution.[23-25] We assume that we formed such species in the early stages of the reaction. However, we were unable to directly characterize the size and structure of the MOC after spin-coating since partial condensation reactions may occur by reacting with atmospheric moisture. These conditions limit the size of the aggregates

of metal-oxo clusters, which is very important for ensuring low surface roughness during the spin coating process and for limiting the line edge roughness after development. In the last step of the solution preparation, 4,4'-Bis(diethylamino)benzophenone (DABP), which is well-known because of its photochemical properties in two-photon absorption[26, 27], was added to the solution. DABP serves as a photo-absorber for two-photon absorption at a wavelength of 800 nm. This compound was also chosen because of its good solubility, which is needed to obtain a homogeneous distribution of the photo-absorber inside the thin film.

After ageing for 24 hours, the solution was casted by spin-coating it on a glass slide. After a pre-baking process (100 °C, 10 s) to remove the solvent from the thin film, the sample was directly introduced into a chamber, enabling control of the atmosphere during the DLW fabrication process. With this setup, the fabrication process was carried out either under air or a pure nitrogen atmosphere. Irradiation was accomplished using a femtosecond laser with an adjustable irradiation time and power. After irradiation, the samples were developed over 20 s in cyclohexanone to remove the non-irradiated part, which revealed the microstructures. For electrical characterizations, the microstructures were connected to gold electrodes deposited by Au sputtering with shadow masks.

We first investigated the effect of femtosecond laser irradiation on the MOC thin film under various laser powers. In this first set of experiments, laser irradiation was conducted in air. **Figure 2a** shows a SEM image of the line structures with different exposure powers. The formulation can be successfully patterned using femtosecond irradiation. For the chosen irradiation time (10 ms for each pixel), crosslinking is obtained for any laser power greater than 10.0 mW. It is observed that the line width increases along with the increase of the exposure power. A width of approximately 650 nm is obtained for the lowest power (10.0 mW). For the highest power (16.5 mW), the width increases to 3 μm. The line edge roughness is limited and continuous lines were obtained for lower and higher powers. For intermediate powers, irregularities within the line pattern were systematically observed. Interestingly, such

defects were obtained with conditions corresponding to the maximum release of organic functions from the thin film. Elimination of organic molecules could provoke this roughness. For higher power, further densification and crystallization smooth the surface of the patterns.

The initial thickness of the film was set to 500 nm by adjusting the spin-coating parameters (from ellipsometry measurements). At low power (10 mW), AFM revealed a height of the lines of 350 nm. At highest power (16.5 mW), the thickness decreased to 80 nm. Such values correspond to a vertical shrinkage of 30 % and 85 % respectively, that corresponds to elimination of organic molecules and densification by condensation and crystallization.

These structures were analyzed using Raman spectroscopy to monitor the chemical modification induced by the laser (**Figure 2b**). The first spectrum is related to the film deposited without any laser treatment. Peaks at 1420, 1594 and 1638 cm^{-1} are visible. From previous studies on metal oxo clusters stabilized by MAA,[14, 28] these peaks were assigned to the MAA linked to Ti. More specifically, these peaks were assigned to $\upsilon_s(COO^-)$, $\upsilon_{as}(COO^-)$ and $\upsilon(C=C)$, respectively.[29] For the low power exposure (10.0 mW), a significant decrease of these peaks was observed, which was attributed to the cleavage of the metal to ligand bond and the release of MAA. Note that this power corresponds to the minimum value to obtain sufficient crosslinking for obtaining stable microstructures on the substrate. With the increased exposure power from 13.2 mW to 16.5 mW, new peaks appeared. The peaks at 435 and 610 cm^{-1} indicated the presence of the rutile phase (R mark in Figure 2b).[30, 31] Two other peaks at 1360 cm^{-1} and 1597 cm^{-1} were attributed to the disordered carbon peaks at the D band and G band, respectively.[32, 33] Usually, the D band is positioned at 1325 cm^{-1}. However, a shift of approximately 35 cm^{-1} was found in the Raman spectrum, which was attributed to the formation of the Ti-O-C bond.[34] It was also observed that the disordered carbon peaks had significantly decreased with the increased exposure power, which was explained by the oxidation of the carbon species under high laser fluency in the presence of oxygen from air. This point will be further discussed below.

The evolution of the Raman spectra with the laser power follows a similar trend to a thermal treatment with an increasing temperature. To verify this point, thin films with the same compositions and thicknesses were prepared in another experiment and were heated in a furnace at different temperatures from 200 °C to 800 °C (1 hour). **Figure 2c** shows the Raman spectra of the Ti-MAA thin film annealed at different temperatures. After annealing at 200°C, a significant decrease of the peaks at 1420, 1594 and 1638 cm^{-1} was observed. As expected, this evolution corresponds to the crosslinking of the Ti-oxo clusters due to thermally induced condensation. This peak evolution is thus similar to that recorded at 10.0 mW, which indicates that laser irradiation under these conditions has the equivalent effect as thermal annealing at 200 °C (1 hour). It was then evaluated whether the decrease of Raman peaks could not be assigned only based on the evaporation of free ligand. For this evaluation, temperature programmed desorption-mass spectroscopy (TPD-MS) was performed on the Ti-MAA thin film. As shown in **Figure S1a**, no strong desorption peak was found below 300 ˚C except for a small amount of water molecules. A group of high desorption peaks at approximately 400 ˚C was attributed to the thermal decomposition of organic compounds into gaseous substances.[7] The above results indicated that the decrease of the Raman peak at 200 ˚C was attributed to the condensation process of Ti-MAA. The above results also showed that the excess MAA that was not bonded to the metal was eliminated during spin-coating. With the increase of the annealing temperature to 500 °C and 800 °C , the peaks corresponding to the anatase phase (A mark) and those of the rutile phase (R mark) were found, as expected.

Microstructures were prepared by two photon structuration (TPS) with the Ti-MAA precursor to evaluate the structural performance and demonstrate the applicability of the DLW approach. The crystallized TiO_2 microstructures (**Figure 2d)** and hybrid organic/TiO_2 microstructures (**Figure 2e)** were fabricated at a high exposure power (16.5 mW) and low exposure power (10 mW), respectively. From the SEM and AFM images, high reproducibility and low surface roughness were observed, highlighting the potential to combine this method with TPS for

creating arbitrary structures with tunable compositions by simply adjusting the fabrication parameters.

These results demonstrate that the thin film formed from the titanium precursor can be successfully patterned at the microscale and that the final material composition can be tuned by changing the laser power. Depending on this parameter, the hybrid material, amorphous TiO_2 or crystallized TiO_2 microstructures that are eventually doped with carbon, can be obtained in a single step at room temperature without any further post-treatment step.

At this stage, the presence of carbon did not lead to conduction, as shown in **Figures S1b** and **S1c**, even when using the photonic parameters that led to the maximum concentration of carbon from the Raman data. This result reveals that the amount of carbon is not sufficient to create a continuous conductive network. As stated before, we assume that C is generated by the graphitization of the organic compounds embedded in the thin film due to laser irradiation. Graphitization of the organic compounds is achieved at an intermediate laser power, which does not result in more C but in the oxidation of CO_2 because of the presence of oxygen in the surrounding atmosphere.

To verify this assumption, laser fabrication was investigated in an oxygen free environment. The samples were fabricated with the same exposure conditions as those in **Figure 2** but in a nitrogen atmosphere by purging the chamber with a continuous N_2-gas flow to reduce the oxidation of carbon. Raman analysis on these samples was performed, and the results are shown in **Figures 3a** and **3b**. **Figure 3a**, which include an additional sample prepared only with thermal annealing at 900 ˚C for 1 hour in a nitrogen atmosphere for comparison. First, we observed that laser microstructuring is still possible under nitrogen. Significant differences in the material structures are evidenced by Raman spectroscopy, especially for the highest powers. The main difference is the large increase of the carbon content, as revealed by the clearly distinguishable D and G band peaks that are present under all conditions, including at the highest power. These two peaks are also present in the sample cured at 900 °C under

nitrogen. Interestingly, the peaks of crystalline TiO_2 could barely be identified, unlike in laser irradiation in air. According to a previous study by Jin et al., the formation of a considerable amount of carbon is able to constrain the crystallization of TiO_2.[35] Another hypothesis relies on the lack of oxygen atoms in the thin film to reach the stoichiometric ratio. To further understand the effect of two-photon irradiation on the graphitization degree (defined as the D/G band ratio)[36-38], we normalized the carbon peaks with the intensity of the G band, as shown in **Figure 3b**. Along with the increase of the exposure power, the relative intensity of the D band decreases. This result indicates a greater degree of graphitization for the highest laser power. We assume that as the laser power is increased, the graphitization is favored. Interestingly, the graphitization degree generated by laser irradiation at a high power (0.64) is better than that of thermal annealing at 900 °C (0.87). To further investigate the structure of the carbon phase, electrical measurements of the TiO_2/carbon composite lines were performed using a two-probe system. As shown in **Figures S2a** and **S2b**, the lines that were fabricated at a low exposure power, from 10 mW to 11.5 mW, revealed no significant conductivity. When the exposure power was increased to 12 mW, the current level was increased, meaning that a continuous carbon network was created within the TiO_2 matrix. The typical Ohm's characteristics were obtained. The resistivity of the lines were evaluated using Ohm's law (**Figure 3c**).[39] The resistance was calculated from the slope of the I-V curve, and the aspect ratio was determined according to the AFM image and gap between the two electrodes (100 μm). A significant decrease of the resistivity was obtained when increasing the exposure power. This behavior is in agreement with the trend of the D/G ratio revealed by the Raman spectra, thus indicating a relation between the nature of the carbon phase and the resistivity of the material. Nevertheless, due to the insulating host TiO_2 matrix, the lowest resistivity of the nanocomposite line exhibited a slightly higher resistance than that of the pure disordered carbon.[40-42]

Conversely, it should be mentioned that another mechanism may account for the significant increase of the conductivity of the material after laser treatment under a nitrogen atmosphere. The partial reduction of TiO_2 into TiO_{2-x} may also occur in the presence of C. This behavior was described by Lu et al..[43] The introduction of oxygen deficiencies with the resultant formation of TiO_{2-x} is known to increase the electrical conductivity.[44]

Figure 3d shows SEM images of the TiO_2/carbon composite structures. The process described here enables the use of DLW to generate well-defined micropatterns of TiO_2 with the inclusion of graphitized carbon leading to conductive properties. It has to be mentioned that the resolution of the structures is slightly degraded compared to that at a lower power. The typical structure width was approximately 4 μm, which was probably due to the lateral heat spreading after laser irradiation.

Room temperature one-step photopatterning is thus achieved with the *in situ* formation of the conductive carbon phase. Moreover, this conductive phase combined with the insulating matrix can potentially exhibit piezoresistive properties and can thus be used as a pressure sensor. To demonstrate this concept, 10 lines connected with two gold electrodes (**Figure 4a**) were prepared following the previously described method. An exposure power of 16.5 mW in a nitrogen atmosphere results in a TiO_2/carbon composite. A controlled pressure was applied by a mechanical performance testing system. A small glass coverslip was added on the top of the microstructure (**Figure S3a**). Because the coverslip was wider than the microstructures, it ensured that a homogeneous force was applied and also avoided the lateral movement of the needle, which might cause scratches on the surface and further damage the structure. Several tests on the pressure sensor were then performed to characterize the piezoresistive response. As shown in **Figure 4b**, the output current signals under different forces from 0 to 1 N display a linear and dynamic response, indicating an instantaneous recovery of the pressure sensor to the loading-unloading of the pressure. To further confirm the reliability, 30 cycles of dynamic forces with different values ranging from 0.2 to 2.4 N were applied to the sensor. The

responses of the pressure sensor to the applied forces for several cycles are shown in **Figure 4c**. A good repeatability of the sensing response in the linear and saturation regimes was observed, demonstrating a stable sensing system without degradation. Nevertheless, the stiffness of the microstructure is also important for the pressure sensor due to the possibility of having a huge force be accidentally applied. Therefore, we investigated the stiffness of the pressure sensor by gradually applying a force up to 3 N corresponding to two times the maximum response force in the linear regime, as shown in **Figure 4d**. A stable response plateau in the saturation regime and an accurate recovery curve after unloading were observed. These results indicated the strong stiffness of our microstructure, which might be attributed to the good mechanical properties of the metal oxide network within our hybrid material structure.

The results show the good dynamic responses and reliability of the pressure sensor with no hysteresis. However, because of the use of the coverslip, the precise value of the applied pressure and sensitivity could not be defined due to the unknown contact area. Therefore, another experiment performed with an atomic force microscope was conducted to define the value of the applied pressure, as shown in **Figure 4e**. The samples were prepared in a single line structure with a width of 5.5 μm. A special large plateau AFM tip with a circular flat top that was 10 μm in diameter and a calibrated stiffness was used to apply the pressure. Thus, the contact area was defined as shown in **Figure S3b**. The tip gradually approached the sensor, and five load/unload cycles were performed, as shown in **Figure 4f**. It is noted that during the AFM approach, according to the default parameters of the AFM system, the cantilever will keep approaching until reaching a certain position, and then, after a small withdrawal, five load/unload cycles will be started. The pressure (P) can be calculated with the following equation: $P = (V*D*K)/A$, where V is voltage of the AFM deflection signal; D and K denote the deflection and spring constant of cantilever, respectively; and A is the contact area. The

applied force was evaluated to be in the range of 23.9 Pa. The sensing of this range of pressure shows the sensitivity at the microscale from a single line. A repeatable response was observed. The sensitivity could be calculated as 0.186 kPa^{-1} based on the definition of $S = (\Delta I/I_0)/P$. This value is comparable to the device responses fabricated by other means [45-48], which shows the great potential of this new fabrication technique.

A possible pressure sensing mechanism of TiO_2/C composite was proposed. At the nanoscale, as schematically illustrated in **Figure 4g**, the pressure applied on the microstructure leads to the compression of the structure. As a result, a diminution of the conductive pathway is expected, thereby leading to a wider conductive network.[49]

Interestingly, while approaching the tip, a negative response was observed slightly before the contact point. This response could be explained by the attractive Van der Waals forces that are applied at a long distance in the approach step, thus causing a snap of the AFM tip at the surface.[50, 51] It demonstrates the sensitivity of the pressure sensor to the attractive forces with a high sensitivity since the force was evaluated at 150 pN.

This set of experiments demonstrates that the material prepared by femtosecond DLW can be used for monitoring forces with good sensitivity and reliability. The fabrication process allows for the preparation of miniaturized pressure sensors at well-defined positions or in high density arrays without thermal curing, which can be useful for applications in artificial skin or cell mechanical response investigations.

To conclude, a new strategy to produce TiO_2 or TiO_2/carbon microstructures using the direct laser writing process was proposed. By changing the laser power and surrounding atmosphere, it is possible to tune the final material composition and confer conductive and piezoresistive properties to the material. The on demand design of complex microstructures is possible due to the laser writing approach. This process greatly simplifies the integration of these materials for the future fabrication of complex devices. The use of femtosecond laser irradiation associated with a two-photon absorption pathway allows the microscale resolution to be

reached. The minimum line width was 650 nm. With experimental conditions needed to obtain crystallized TiO_2 and TiO_2/C, typical line widths were 3 μm. Pressure sensors were chosen to illustrate the potential applications of such an approach. Other applications for energy storage, solar cells or photocatalysis can also be developed from these results.

Experimental Section

Preparation of Solutions: One milliliter of titanium($_{IV}$) tetraisopropoxide ($C_{12}H_{28}O_4Ti$, Sigma-Aldrich) and 2 mL of methacrylic acid (99%, Sigma-Aldrich) were mixed together and stirred for 5 min. Then, 2 mL of 1-propanol (anhydrous grade, 99.7%, Sigma-Aldrich) was added as a solvent and stirred for another 10 min. After that, 0.9 mL of acidified water (HCL, 0.37 $_M$) was introduced into the solution. After 24 h of vigorous stirring, 1 wt% (to titanium precursor) of DABD (4,4'-Bis(diethylamino)benzophenone, Sigma-Aldrich) was finally added as a photo-absorber before use. The typical formulation composition was thus Ti:MAA:H_2O:solvent = 1:7:15:8.

Two-photon fabrication of TiO_2 structure: The solution was filtered through a 0.2 μm pore diameter filter and spin-coated on a glass substrate to obtain a xerogel film with a thickness of approximately 500 nm. A pre-baking step was used between spin-coating and laser irradiation (100°C, 10 sec) to remove the solvent from the thin film. The sample was directly transferred to a special chamber holder to control the atmosphere during fabrication. In particular, the chamber could be filled with dry nitrogen. For the microfabrication, we used a commercial set-up purchased from Microlight based on 3D direct laser writing technology. Thanks to this no mask technology, arbitrary and complex 2D and 3D shapes can be easely fabricated with 0.2 to 3 microns resolution in the x,y plane. This 3D microprinting machine include a standard microscope (Zeiss Observer D1), a piezo stage (PI Mars 300 μm^3) a sub-ns microlaser (TeemPhotonics) and a dedicated software to optimize fabrication paths and to

control the machine. However, in this study, to favor the two-photon absorption process from the chosen dye, we have replaced the sub-ns source by a femtoseond laser source (Chameleon Ultra II, 140 fs @ 800 nm). The laser beam was introduced via a 40X objective (NA: 0.65), and the exposure time was set to 10 ms with different exposure powers from 10 mW to 16.5 mW. The beam diameter was evaluated to 750 nm. The local dose is thus comprised between 0.10 to 0.16 mJ and the surface energy between 22.6 and 37.3 kJ/cm^2. After the laser exposure, the sample was developed by immersion in cyclohexanone for 20 s and dried by N_2 purging.

Micro Raman Spectroscopy Analysis: The preparation of samples for thermal annealing was performed by spin-coating the solution onto a quartz substrate and annealing it in a furnace. To monitor the laser induced modifications, the DLW system was used to fabricate a square structure with dimensions of 30x30 μm^2. Then, micro Raman spectroscopy analysis was conducted using a Spectrometer Labrum HR with a 532 nm excitation laser and CCD detector. The Raman signals were acquired in a backscattering configuration with a 100X objective.

Characterization Methods: An SEM (Quanta 400 FEL) and an AFM (Picoplus 5500 Agilent) in resonant mode were used to characterize the samples in this study. For SEM characterization, a thin layer of Au around 10 nm was sputtered on samples.

Temperature Programming Desorption – Mass Spectrometry (TPD-MS) Analysis: To investigate the degradation of the spin-coated thin film, a homemade temperature-programmed desorption coupled to a mass spectrometry setup was used. For the detailed description of the TPD-MS, one can refer to our recently published paper. [15]

Fabrication and Electrical measurement of TiO_2/Carbon structure: Two gold electrodes with a distance of 100 μm were first sputtered onto a clean glass substrate using a shadow mask. Then, the solution was spin-coated onto the glass substrate. Using DLW process, 10 lines with a width of approximately 5.5 μm were fabricated between the two electrodes. The electrical performance was measured using a digital source meter (Keithley 2636B).

Performance test of TiO_2/Carbon Pressure Sensor: To apply a controlled force to the substrate, a mechanical performance testing system (Lhomargy DY 34) was used. The electrical response of the sensor was recorded with a digital source meter (Keithley 2636B). The samples were prepared in the same way as those for the electrical measurements. A needle was used to apply the force in a confined area, and a small glass substrate was placed beneath pressure sensor to ensure that a homogeneous force was applied and to protect the structure. The sensor was operated with a voltage of 3 V to record the changes of the current. For the microscale pressure tests, a force AFM (Nanosurf C3000) was used to apply pressure with a specially designed flat top AFM tip (Nanosensors SD-PL-NCH-SPL). The diameter of this flat top tip was 10 μm. The pressure (P) was defined as $P = (V*D*K)/A$, where V is the deflection voltage of the AFM deflection signal; D and K denote the deflectivity and spring constant of the cantilever, respectively; and A is the contact area. In the task, five repetitions with a deflection voltage of 0.001 V were performed. By knowing the D and K values of the cantilever (125 nm/V and 10.5 N/m, respectively), a pressure of 23.86 Pa was calculated.

Supporting Information
Supporting Information is available from the Wiley Online Library or from the author.

Acknowledgements
The authors would like to thank Patrick Lamielle for designing gaz control chamber, and Simon Gree for helpfull discussion regarding the Raman microspectroscopy. This work was supported by funding from Agence Nationale pour la Recherche (Project PHOTOMOC, ANR-14-CE26-0039 & Project 2PhotonInsight, ANR-16-CE08-0020), Région Grand Est (MIPPI 4D) and Ministry of Science and Technology, Taiwan (Project 104-2923-E-009-001-MY3).

Received: ((will be filled in by the editorial staff))
Revised: ((will be filled in by the editorial staff))
Published online: ((will be filled in by the editorial staff))

References

[1] Y. H. Kim, J. S. Heo, T. H. Kim, S. Park, M. H. Yoon, J. Kim, M. S. Oh, G. R. Yi, Y. Y. Noh, S. K. Park, *Nature* **2012**, 489, 128.

[2] S. B. Ogale, T. V. Venkatesan, M. Blamire, *Functional Metal Oxides: New Science and Novel Applications*, Wiley-VCH, Weinheim, Germany **2013**.

[3] E. Comini, *Mater. Today* **2016**, 19, 559.

[4] B. K. Sharma, J. H. Ahn, *Adv. Electron. Mater.* **2016**, 2, 17.

[5] C.-C. Yeh, H.-W. Zan, O. Soppera, *Advanced Materials* **2018**, 0, 1800923.

[6] F. Stehlin, Y. Bourgin, A. Spangenberg, Y. Jourlin, O. Parriaux, S. Reynaud, F. Wieder, O. Soppera, *Opt. Lett.* **2012**, 37, 4651.

[7] C.-C. Yeh, H.-C. Liu, M.-Y. Chuang, J. Denzer, D. Berling, H.-W. Zan, O. Soppera, *Advanced Materials Interfaces* **2016**, 3, 1600373.

[8] Y. Wang, I. Fedin, H. Zhang, D. V. Talapin, *Science* **2017**, 357, 385.

[9] H. Palneedi, J. H. Park, D. Maurya, M. Peddigari, G.-T. Hwang, V. Annapureddy, J.-W. Kim, J.-J. Choi, B.-D. Hahn, S. Priya, K. J. Lee, J. Ryu, *Advanced Materials* **2018**, 30, 1705148.

[10] T. Nakajima, K. Shinoda, T. Tsuchiya, *Chemical Society Reviews* **2014**, 43, 2027.

[11] A. Queraltó, A. Pérez del Pino, M. de la Mata, J. Arbiol, M. Tristany, X. Obradors, T. Puig, *Chemistry of Materials* **2016**, 28, 6136.

[12] J. Yeo, S. Hong, M. Wanit, W. Kang Hyun, D. Lee, P. Grigoropoulos Costas, J. Sung Hyung, H. Ko Seung, *Advanced Functional Materials* **2013**, 23, 3316.

[13] J. Yeo, S. Hong, G. Kim, H. Lee, Y. D. Suh, I. Park, C. P. Grigoropoulos, S. H. Ko, *ACS Nano* **2015**, 9, 6059.

[14] F. Stehlin, F. Wieder, A. Spangenberg, J.-M. Le Meins, O. Soppera, *Journal of Materials Chemistry C* **2014**, 2, 277.

[15] H. Segawa, N. Abrams, E. Mallouk Thomas, I. Divliansky, S. Mayer Theresa, *Journal of the American Ceramic Society* **2006**, 89, 3507.

[16] C.-C. Yeh, H.-C. Liu, W. Heni, D. Berling, H.-W. Zan, O. Soppera, *Journal of Materials Chemistry C* **2017**, 5, 2611.

[17] H. Segawa, S. Matsuo, H. Misawa, *Applied Physics A* **2004**, 79, 407.

[18] Z. X. Chen, W. X. Wang, Y. Takao, T. Matsubara, L. M. Ren, *Applied Surface Science* **2011**, 257, 7254.

[19] N. Wu, J. Wang, D. N. Tafen, H. Wang, J.-G. Zheng, J. P. Lewis, X. Liu, S. S. Leonard, A. Manivannan, *Journal of the American Chemical Society* **2010**, 132, 6679.

[20] F. Sauvage, F. Di Fonzo, A. Li Bassi, C. S. Casari, V. Russo, G. Divitini, C. Ducati, C. E. Bottani, P. Comte, M. Graetzel, *Nano Letters* **2010**, 10, 2562.

[21] Q. Zheng, B. Zhou, J. Bai, L. Li, Z. Jin, J. Zhang, J. Li, Y. Liu, W. Cai, X. Zhu, *Advanced Materials* **2008**, 20, 1044.

[22] Y. Wang, J. Miao, Y. Tian, C. Guo, J. Zhang, T. Ren, Q. Liu, *Opt. Express* **2011**, 19, 17390.

[23] F. Babonneau, J. Maquet, *Polyhedron* **2000**, 19, 315.

[24] H. Ridaoui, F. Wieder, A. Ponche, O. Soppera, *Nanotechnology* **2010**, 21, 065303.

[25] O. Soppera, C. Croutxé-Barghorn, D. J. Lougnot, *New Journal of Chemistry* **2001**, 25, 1006.

[26] J. Fischer, G. von Freymann, M. Wegener, *Advanced Materials* **2010**, 22, 3578.

[27] A. Ovsianikov, J. Viertl, B. Chichkov, M. Oubaha, B. MacCraith, I. Sakellari, A. Giakoumaki, D. Gray, M. Vamvakaki, M. Farsari, C. Fotakis, *ACS Nano* **2008**, 2, 2257.

[28] E. S. Rufino, E. E. C. Monteiro, *Polymer* **2000**, 41, 4213.

[29] I. Karatchevtseva, D. J. Cassidy, Z. Zhang, G. Triani, K. S. Finnie, S. L. Cram, C. J. Barbé, J. R. Bartlett, *Journal of the American Ceramic Society* **2008**, 91, 2015.

[30] T. Kasuga, M. Hiramatsu, A. Hoson, T. Sekino, K. Niihara, *Advanced Materials* **1999**, 11, 1307.

[31] P. P. Lottici, D. Bersani, M. Braghini, A. Montenero, *Journal of Materials Science* **1993**, 28, 177.

[32] K. Dasgupta, D. Sathiyamoorthy, *Materials Science and Technology* **2003**, 19, 995.

[33] A. C. Ferrari, J. Robertson, *Physical Review B* **2000**, 61, 14095.

[34] X.-P. Liu, D.-D. Song, L. Wan, X.-B. Pang, Z. Li, *Bulletin of Materials Science* **2015**, 38, 1263.

[35] S. Jin, S. Zhang, R. Zhang, M. Jin, *Fullerenes, Nanotubes and Carbon Nanostructures* **2016**, 24, 67.

[36] Y. Lim, J. H. Chu, D. H. Lee, S.-Y. Kwon, H. Shin, *Journal of Alloys and Compounds* **2017**, 702, 465.

[37] M. Vasei, P. Das, H. Cherfouth, B. Marsan, J. P. Claverie, *Frontiers in Chemistry* **2014**, 2, 47.

[38] A. C. Ferrari, *Solid State Communications* **2007**, 143, 47.

[39] Y. Singh, *International Journal of Modern Physics: Conference Series* **2013**, 22, 745.

[40] B. D. Keller, N. Ferralis, J. C. Grossman, *Nano Letters* **2016**, 16, 2951.

[41] A. W. P. Fung, A. M. Rao, K. Kuriyama, M. S. Dresselhaus, G. Dresselhaus, M. Endo, N. Shindo, *Journal of Materials Research* **2011**, 8, 489.

[42] K. Ju-Seung, K. Jong-Uk, S. Chang-Ho, G. Hal-Bon, "The electrical and electrochemical properties of poly(p-phenylene)-based carbon for lithium rechargeable batteries", presented at *Proceedings of 5th International Conference on Properties and Applications of Dielectric Materials*, 25 -30 May 1997, **1997**.

[43] Y. Lu, M. Hirohashi, K. Sato, *MATERIALS TRANSACTIONS* **2006**, 47, 1449.

[44] H. Lee, S. J. Han, R. Chidambaram Seshadri, S. Sampath, *Scientific Reports* **2016**, 6, 36581.

[45] Q. Wang, M. Jian, C. Wang, Y. Zhang, *Advanced Functional Materials* **2017**, 27, 1605657.

[46] S. Parikshit, B. Sushmee, *Nanotechnology* **2017**, 28, 095501.

[47] M. Jian, K. Xia, Q. Wang, Z. Yin, H. Wang, C. Wang, H. Xie, M. Zhang, Y. Zhang, *Advanced Functional Materials* **2017**, 27, 1606066.

[48] G. Schwartz, B. C. K. Tee, J. Mei, A. L. Appleton, D. H. Kim, H. Wang, Z. Bao, *Nature Communications* **2013**, 4, 1859.

[49] G. Y. Bae, S. W. Pak, D. Kim, G. Lee, D. H. Kim, Y. Chung, K. Cho, *Advanced Materials* **2016**, 28, 5300.

[50] W. Zhang, H. Yang, F. Liu, T. Chen, G. Hu, D. Guo, Q. Hou, X. Wu, Y. Su, J. Wang, *RSC Advances* **2017**, 7, 32518.

[51] H. W. Zhang, J. B. Wang, H. F. Ye, L. Wang, *International Journal of Solids and Structures* **2007**, 44, 2783.

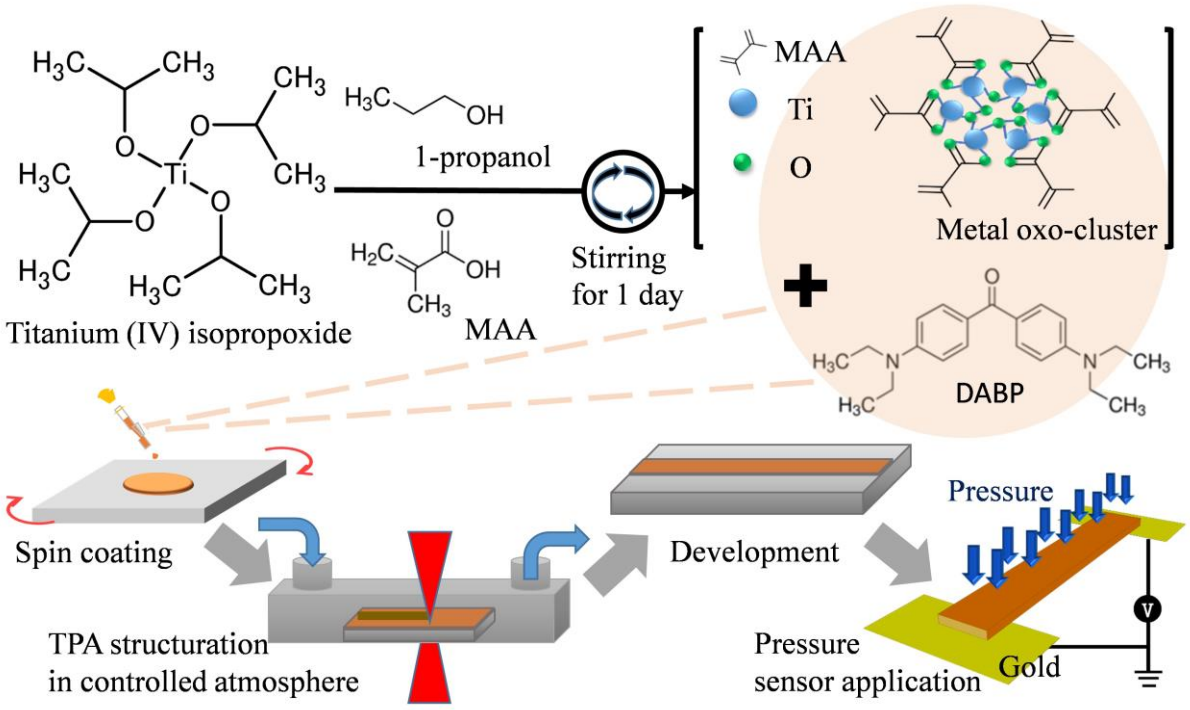

Figure 1. Schematic of the preparation of the solution and the one-step micro pressure sensor fabrication process: Titanium isopropoxide is first chelated with the MAA ligand and a DABP photoabsorber is added. Then, the solution is spin-coated on a glass substrate, irradiated by an NIR femtosecond laser focused beam in a controlled atmosphere and developed in cyclohexanone. Finally, the structure is connected to an electrical circuit, and the electrical properties under a controlled pressure can be monitored.

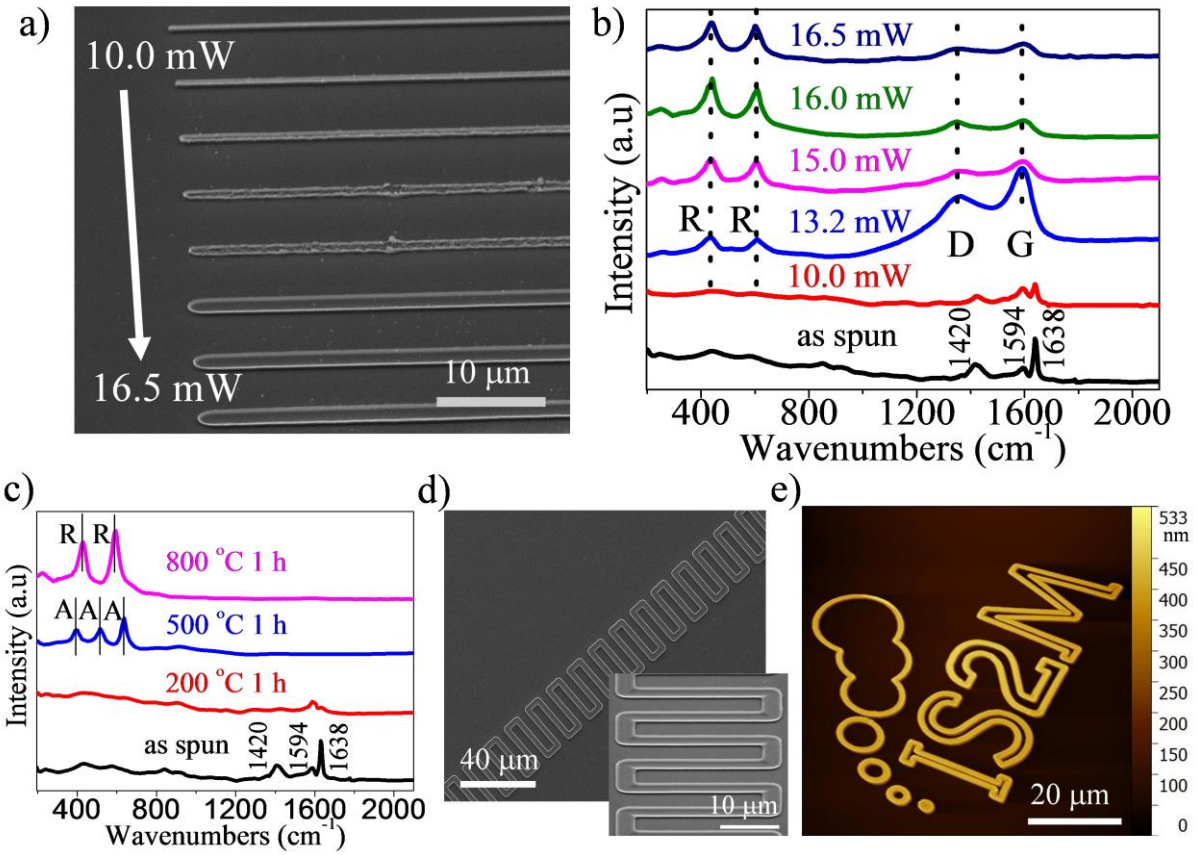

Figure 2. Laser curing in air of the TiO_2 precursor material. a) SEM image of the line structure fabricated with different powers from 10.0 mW to 16.5 mW. b) Raman spectra of the microstructures generated by direct laser writing with different irradiation powers. c) Raman spectra of the spin coated thin film after thermal annealing at different temperatures (1 hour). R and A stand for "Rutile" and "Anatase" in the Raman spectra, respectively. d) Finger type microstructure fabricated at 16.5 mW. e) AFM image of the IS2M logo fabricated under a low exposure power (10.0 mW).

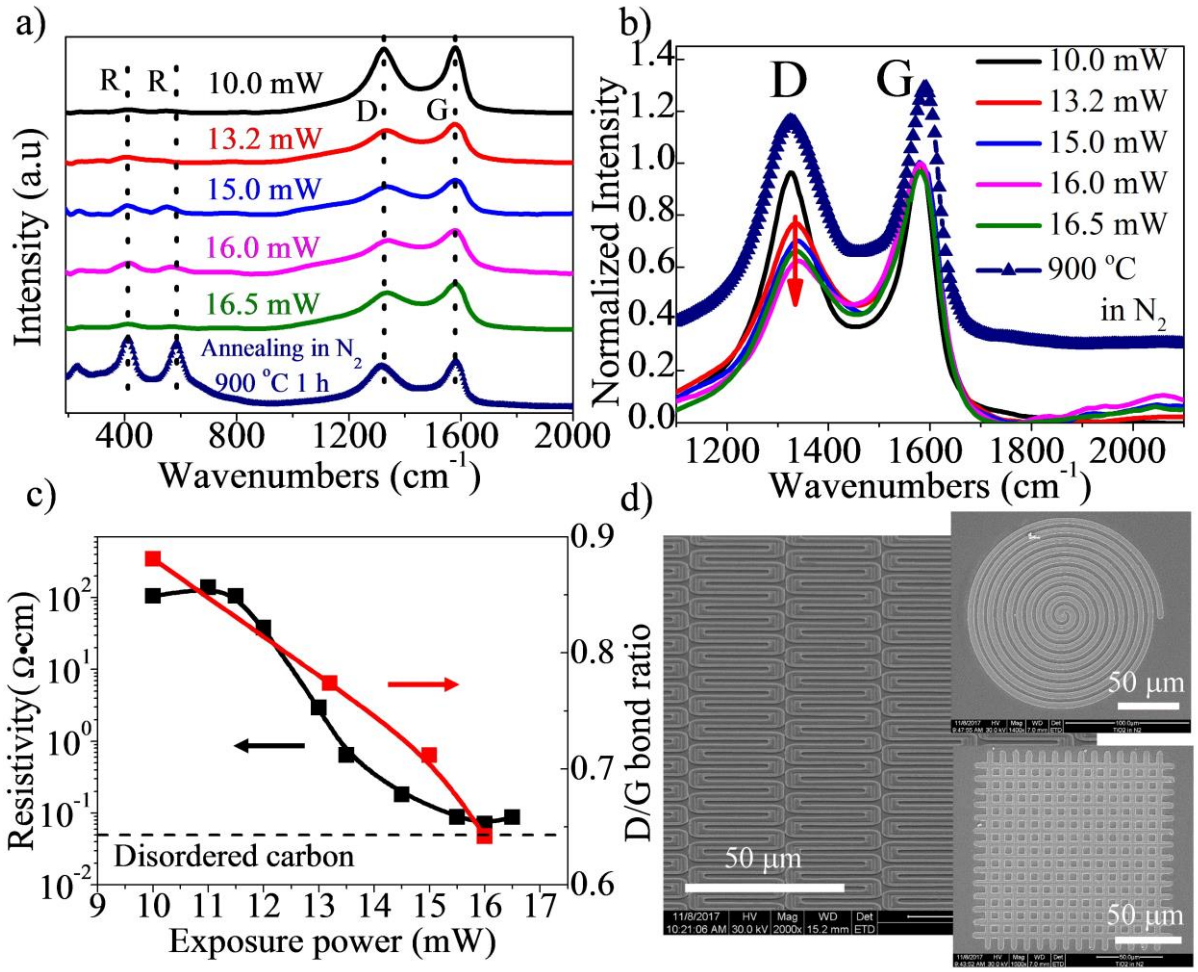

Figure 3. Characteristics of the TiO_2 microstructure generated in a N_2 atmosphere. a) Raman spectrum of the TiO_2 microstructures with different fabrication powers and a spin coated thin film annealed in 900 ˚C 1 h with a vertical shift of 0.3 unit. b) Zoomed in spectra in the range of 1100-2100 cm^{-1} and normalized by the carbon G bond. c) Resistivity and D/G bond ratio plot versus the exposure power of the TiO_2 microstructures. d) SEM image of the arbitrary TiO_2/carbon microstructure generated with 16 mW.

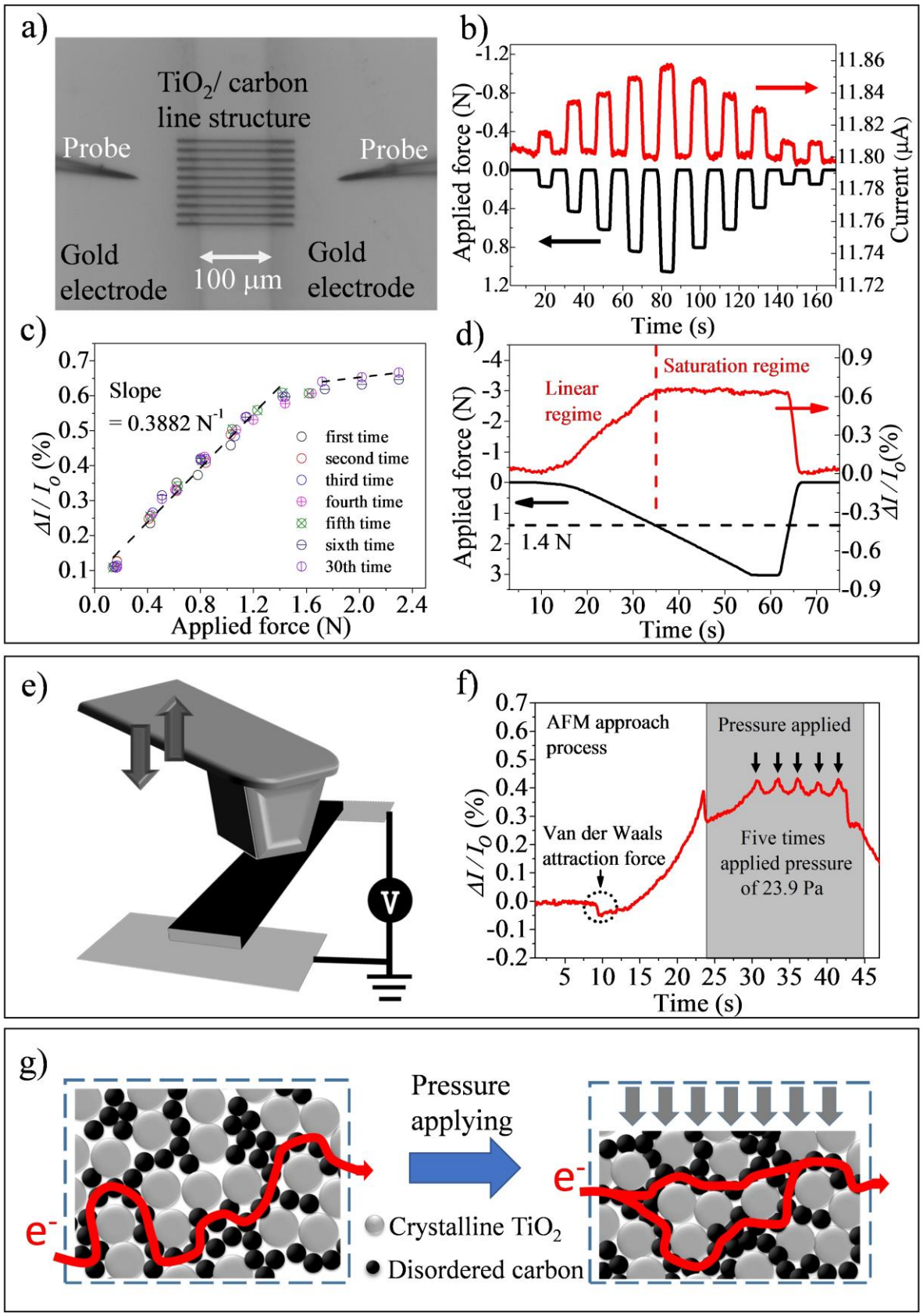

Figure 4. Reliability, sensitivity, durability and mechanism of the TiO_2/carbon composite pressure sensors. a) Optical microscopy image of the TiO_2/carbon microstructure pressure sensor device. b) The change in the current under an applied force ranging from 0.2 N to 1.1

N. c) The sensitivity and reliability of the pressure sensor with 30 cycles of force applied. d) The durability of the pressure sensor with an excess applied force of 3N. e,f) The illustration and response data of the force AFM experiment with five times 23.9 Pa pressure applied, respectively. g) The mechanism of the resistance change in TiO_2/carbon piezoresistive pressure sensor.

Supporting Information

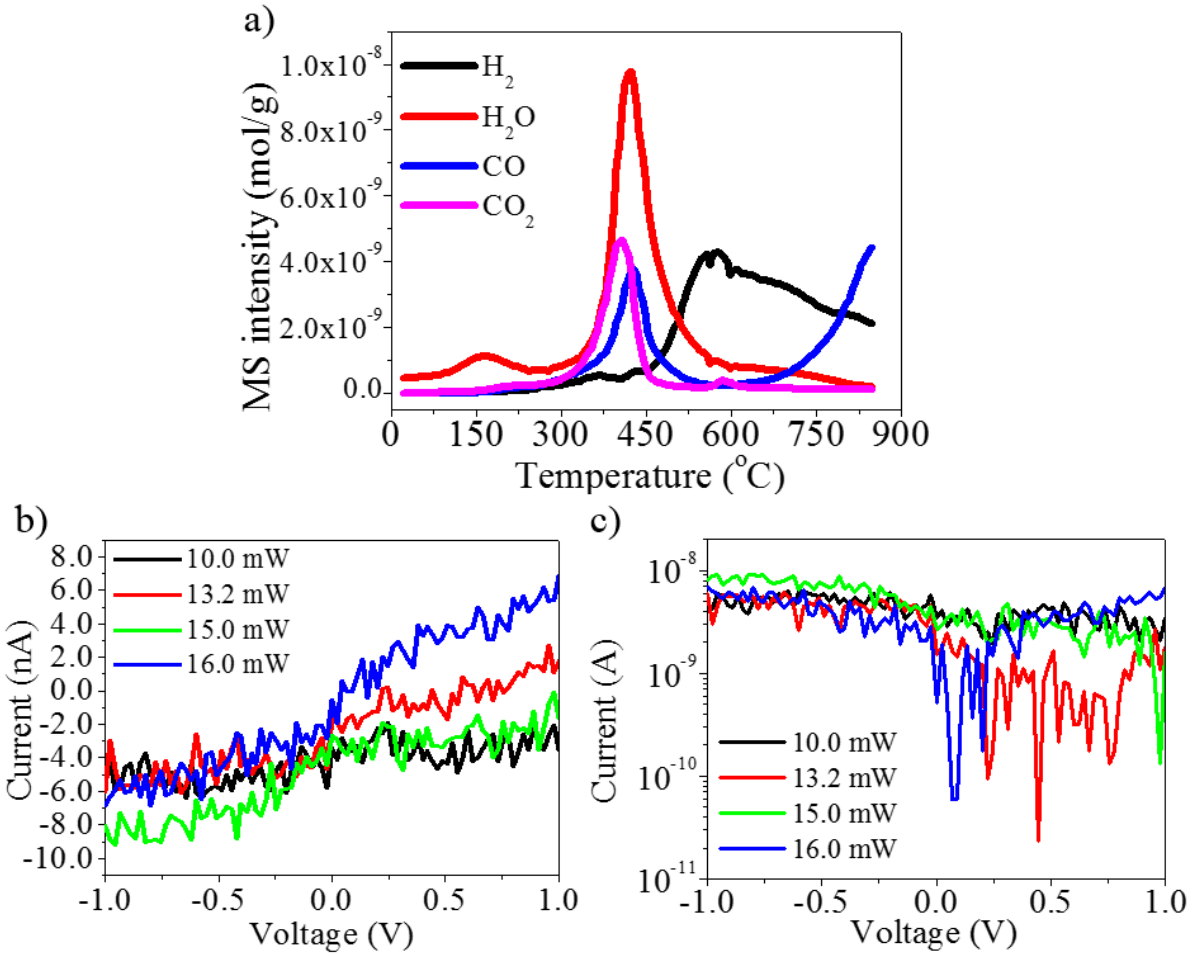

Figure S1. a) TPD-MS spectrum of the spin coated TiMAA gel film. b) and c) Linear and log scale of the I-V curve of TiO_2 line with different exposure powers, respectively.

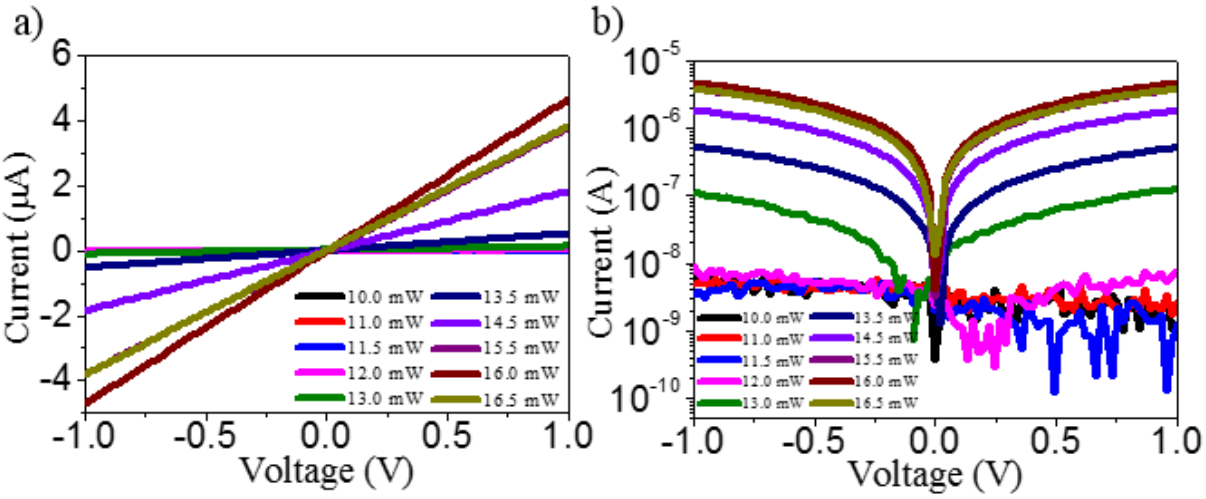

Figure S2. a) and b) Linear and log scale of the I-V curve of TiO_2/carbon line with different exposure powers from 10.0 mW to 16.5 mW, respectively.

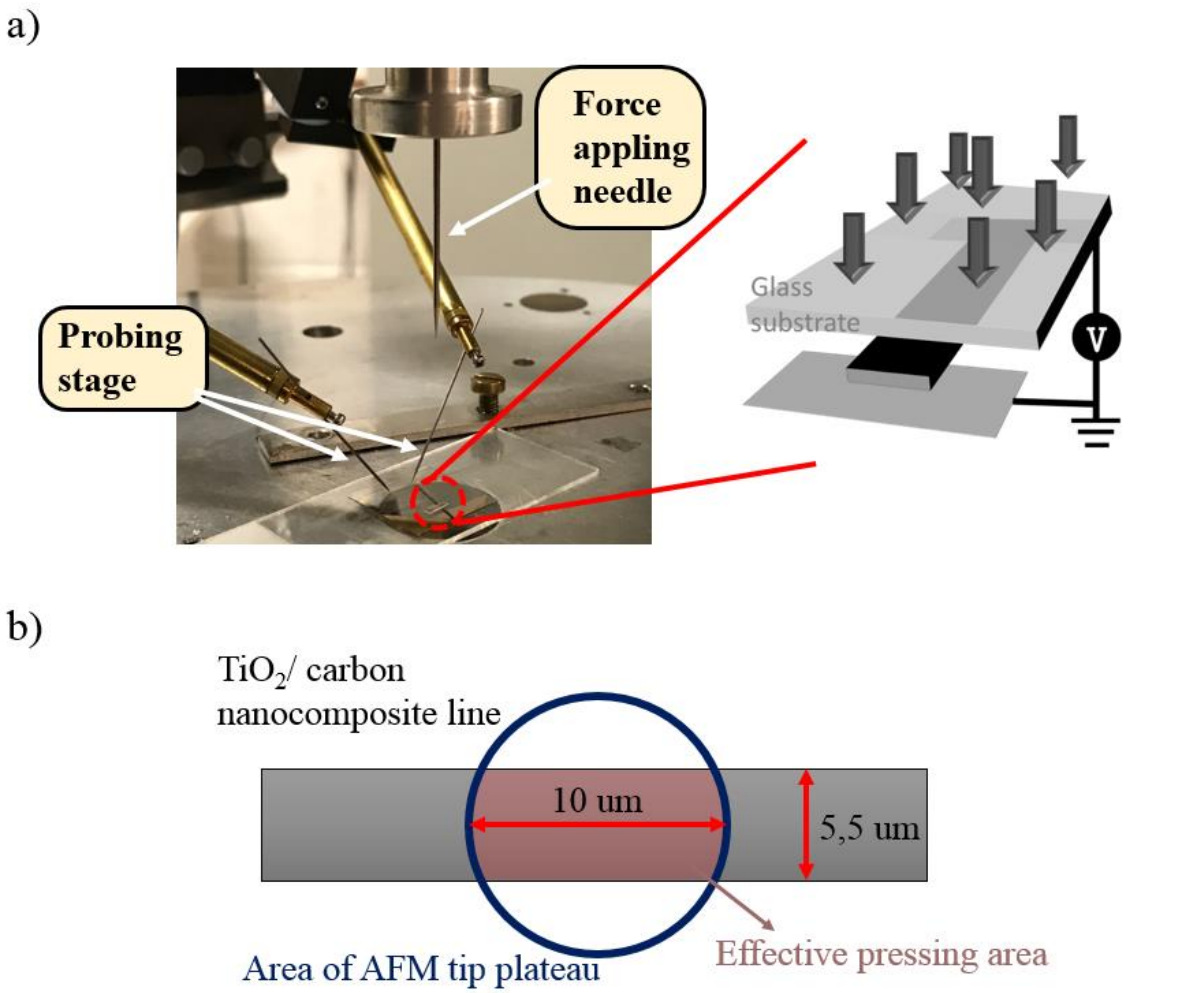

Figure S3. a) Photograph of the setup for applying the force to the device and monitoring electrical measurements. The right panel shows the schematic of the pressure sensor device. b) Schematic of the applied force area on the TiO_2/carbon sensor using an AFM tip.